

# Inverse Currents in Hamiltonian Coupled Transport

Jiao Wang,<sup>1</sup> Giulio Casati,<sup>2,3</sup> and Giuliano Benenti<sup>2,4,5</sup>

<sup>1</sup>*Department of Physics and Key Laboratory of Low Dimensional Condensed Matter Physics (Department of Education of Fujian Province), Xiamen University, Xiamen 361005, Fujian, China*

<sup>2</sup>*Center for Nonlinear and Complex Systems, Dipartimento di Scienza e Alta*

*Tecnologia, Università degli Studi dell'Insubria, via Valleggio 11, 22100 Como, Italy*

<sup>3</sup>*International Institute of Physics, Federal University of Rio Grande do Norte, Campus*

*Universitário - Lagoa Nova, CP. 1613, Natal, Rio Grande Do Norte 59078-970, Brazil*

<sup>4</sup>*Istituto Nazionale di Fisica Nucleare, Sezione di Milano, via Celoria 16, 20133 Milano, Italy*

<sup>5</sup>*NEST, Istituto Nanoscienze-CNR, I-56126 Pisa, Italy*

The occurrence of an inverse current, where the sign of the induced current is opposite to the applied force, is a highly counterintuitive phenomenon. We show that inverse currents in coupled transport (ICC) of energy and particle can occur in a one-dimensional interacting Hamiltonian system when its equilibrium state is perturbed by coupled thermodynamic forces. This seemingly paradoxical result is possible due to the self-organization occurring in the system in response to the applied forces.

In the study of particle transport, inverse particle current, denoted as absolute negative mobility (ANM), is arguably the most counterintuitive transport phenomenon, in that a system responds to an applied static force by generating a current against that force. It has been pointed out that ANM cannot take place around a thermal equilibrium state [1, 2], otherwise it could be exploited to construct a perpetual mobile of the second kind, with a single heat bath performing work. In nonequilibrium systems, however, there is no fundamental law that forbids ANM, and indeed ANM has been investigated in a variety of nonequilibrium setups, e.g., in relation to particle separation [3, 4], self-propulsion [5], tracer dynamics in a steady laminar flow [6], and also experimentally in semiconductor superlattices [7], microfluidic systems [8], and Josephson junctions [9], subject to ac electric fields.

The above argument of a perpetual mobile only applies when there is a single flow in response to a single driving force acting on the system. It does not rule out the possibility of inverse currents in coupled transport (ICC). Indeed, the entropy production rate  $\dot{S} = J_1 \mathcal{F}_1 + J_2 \mathcal{F}_2$ , with  $\mathcal{F}_i > 0$  ( $i = 1, 2$ ) thermodynamic forces and  $J_i$  conjugated currents, can be positive even though one of the two induced currents has sign opposite to both forces (say,  $J_1 > 0$  and  $J_2 < 0$ ). Nevertheless, the possibility that ICC can take place by perturbing an equilibrium state by means of two forces, though not in contradiction with thermodynamics, appears highly counterintuitive. Indeed, it would imply that a system at equilibrium exposed to two thermodynamic forces, could, under appropriate conditions, exhibit ICC *against both forces*. Actually, such a possibility has been recently shown to occur in an abstract stochastic model [10]. More precisely, it was obtained for a stochastic dynamics, with a tracer particle subject to two driving forces and moving on a discrete ring populated by neutral particles, which in turn obey a symmetric exclusion process. However,

such type of ICC has not been shown possible in any physical system. In particular, in the model of hard Brownian disks in a narrow planar chain, of which the above stochastic model serves as a toy model, ICC was not found [10]. It raises the basic question if, besides abstract stochastic models, the ICC phenomenon can take place in a purely dynamical, Hamiltonian system when perturbing its equilibrium state.

In this Letter we give a positive answer to this question by considering a one-dimensional (1D), two masses, interacting gas model. It is found that by perturbing its equilibrium state with biases in temperature and chemical potential, it is possible to have one flow (either particle or energy) *against both biases*. This seemingly paradoxical result is possible due to a negative Onsager cross coefficient for thermodiffusion, which in turn is rooted in the surprising property of our model of adapting its structure in response to external gradients, with separation of the two species of particles of different masses [11].

Our model can be viewed as a classical version of the Lieb-Liniger model [12] for a diatomic gas. A schematic drawing is provided in Fig. 1, where the two species of particles of mass  $\mathcal{M}_1$  and  $\mathcal{M}_2$  are denoted as bullets and rods, respectively, for visualization purposes. The masses are confined to move in a 1D box of length  $L$ , with the Hamiltonian

$$H = \sum_i \frac{p_i^2}{2m_i} + \sum_{i < j} V(x_i - x_j). \quad (1)$$

Here  $m_i \in \{\mathcal{M}_1, \mathcal{M}_2\}$ ,  $p_i$ , and  $x_i$  are, respectively, the mass, momentum, and position of the  $i$ th particle, and the potential  $V(x) = h$  for  $x \leq |r|$  and  $V(x) = 0$  otherwise, with  $h \geq 0$  being the potential barrier.

In this work we consider the limit  $r \rightarrow 0$  where all particles move freely except when two particles meet. At such a moment, the two particles simply pass through each other if their total energy in the frame of the center of mass is larger than the potential barrier  $h$ ; otherwise

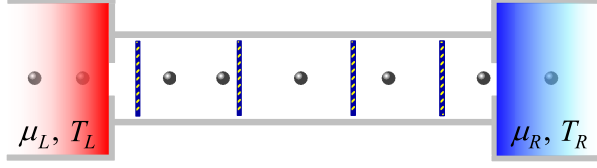


FIG. 1. Schematic drawing of the 1D, two mass, interacting gas model. It consists of a diatomic gas of particles which, for visualization purposes, we represent by bullets and rods, respectively. The system is coupled to two reservoirs at its two ends, with which the rods exchange energy while the bullets exchange both energy and particles.

they collide elastically. Note that for  $h = 0$ , interactions vanish and the system is integrable. For  $h = \infty$ , the system reduces to the nonintegrable, hard-core two-mass gas [13], an intensively studied paradigm for the 1D transport problem. Interestingly, for a finite nonzero value of  $h$ , the system's transport behavior is very rich [11, 14]. In particular, as shown in Ref. [11], when the system is brought into contact with two heat baths at different temperatures, it may undergo a nonequilibrium phase transition as the temperature difference increases.

In the following we investigate a different setup where also the particle current plays a role (see Fig. 1): two reservoirs of one kind of particles, say, the “bullets”, are introduced to replace the heat baths. The reservoirs are modeled as infinite 1D ideal gases [15], which are allowed to exchange both energy and (bullet) particles with the system; i.e., when a bullet particle hits a reservoir, it will be absorbed; meanwhile, the reservoirs inject bullet particles into the system randomly, with rates  $\gamma_\alpha$  ( $\alpha = L, R$ ) determined by their temperatures  $T_\alpha$  and chemical potentials  $\mu_\alpha$  as [16]

$$\gamma_\alpha = \frac{\rho_0}{\sqrt{2\pi\mathcal{M}_1\beta_0}} \frac{\beta_0}{\beta_\alpha} e^{\mu_\alpha\beta_\alpha - \mu_0\beta_0}. \quad (2)$$

Here,  $\beta_0 = 1/(k_B T_0)$  with  $k_B$  the Boltzmann constant, and  $T_0$ ,  $\rho_0$ , and  $\mu_0$  are, respectively, the temperature, particle number density, and chemical potential of a reference state. An injected particle has a random velocity sampled from the distribution [17]

$$P_\alpha(v, \mathcal{M}_1) = \mathcal{M}_1 |v| \beta_\alpha e^{-\mathcal{M}_1 v^2 \beta_\alpha / 2}, \quad (3)$$

and the time interval between two neighboring injections of a reservoir obeys the Poisson distribution  $\dot{P}_\alpha(t) = \gamma_\alpha e^{-\gamma_\alpha t}$ . Instead, the rod particles only exchange energy with the reservoirs; i.e., when a rod particle hits a reservoir, it will be reflected back with a new velocity randomly chosen from  $P_\alpha(v, \mathcal{M}_2)$  [18]. The total number of rod particles is thus conserved.

The system is subject to the thermodynamic forces  $\mathcal{F}_\rho = \mu_L \beta_L - \mu_R \beta_R$  and  $\mathcal{F}_u = \beta_R - \beta_L$ , conjugated to

the particle and energy currents,  $J_\rho$  and  $J_u$ , respectively. We set  $\mathcal{F}_\rho > 0$  and  $\mathcal{F}_u > 0$ , so that a negative current signals ICC. Note that the ICC phenomenon should not be confused with thermodiffusion, where the two thermodynamic forces have opposite sign instead and, for instance, the motion of particles against a chemical potential difference is possible thanks to a temperature difference.

In our numerical simulations, we set  $T_L = T + \Delta T/2$ ,  $\mu_L = \mu + \Delta\mu/2$ ,  $T_R = T - \Delta T/2$ , and  $\mu_R = \mu - \Delta\mu/2$ . We focus on the illustrative example with  $T = 1$  and  $\mu = 1.5$ , but ICC has been verified to be independent of this particular choice. Other parameter values are:  $k_B = 1$ ,  $h = 1$  throughout unless explicitly stated otherwise,  $\mathcal{M}_1 = 1$ , and  $\mathcal{M}_2 = 0.5$  (as explained below, to have ICC it is crucial that  $\mathcal{M}_1 > \mathcal{M}_2$ , that is, the particles exchange with the reservoirs are the heavier ones). The number of rods is set to be half of the expected particle number of a 1D ideal gas at the equilibrium state with given  $T$  and  $\mu$ ; i.e.,  $N_{\mathcal{M}_2} = \rho L/2$  with  $\rho = \rho_0 (\sqrt{\beta_0/\beta}) e^{\beta\mu - \beta_0\mu_0}$ . (For the reference state,  $\rho_0 = 1$ ,  $T_0 = 1$ , and  $\mu_0 = 0$ .) To evolve the system, an effective event-driven algorithm is utilized [19] to ensure the relative errors of all numerical results are smaller than 0.5%.

We start by seeking ICC in the simpler cases when only one thermodynamic force acts. First, we set  $\mathcal{F}_\rho = 0$  to see how the currents depend on the force  $\mathcal{F}_u$ . A typical result is shown in Figs. 2(a) and 2(b), where it is seen that while  $J_u$  is positive and monotonically increases with  $\mathcal{F}_u$ ,  $J_\rho$  is negative and decreases with increasing  $\mathcal{F}_u$ , until it reaches a turning point. This is a clear evidence of ICC, since over the whole range of  $\mathcal{F}_u$  investigated  $J_\rho$  is negative, i.e., the particle current flows from the low to the high temperature reservoir. Note that for small  $\mathcal{F}_u$  ( $< 0.3$  in this case) both currents depend on  $\mathcal{F}_u$  linearly, suggesting that the system is in the linear response regime. Therefore, as indicated by Fig. 2(a), ICC can take place in both the linear response regime and beyond.

Similarly, a parallel study reveals how the currents depend on the thermodynamic force  $\mathcal{F}_\rho$  with  $\mathcal{F}_u = 0$  [see Figs. 2(c) and 2(d)]. Again, ICC is observed, but in the energy current  $J_u$  instead, i.e., the energy flows from the reservoir of the lower chemical potential to the opposite one (note that here the two reservoirs have the same temperature since  $\mathcal{F}_u = 0$ ).

In order to have an overall grasp of how the currents depend on the thermodynamic forces, we thoroughly compute the currents for various  $\mathcal{F}_\rho$  and  $\mathcal{F}_u$ . The results are summarized in Fig. 3. An area of  $(\mathcal{F}_\rho, \mathcal{F}_u)$  for ICC in the particle current  $J_\rho$  can be recognized in Fig. 3(a) (above the white dashed line), while the ICC in the energy current  $J_u$  can be found in Fig. 3(b) (below the white dashed line). The two ICC areas do not overlap, as expected, since simultaneous ICC in both currents would lead to a negative entropy production rate, thus violating the second law of thermodynamics.

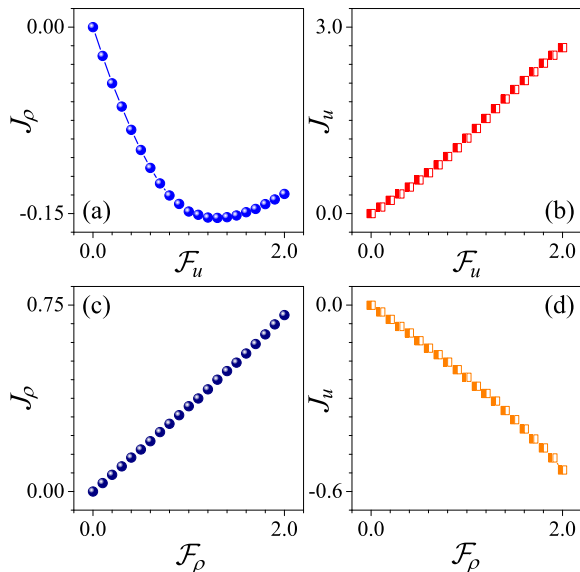


FIG. 2. The particle current  $J_\rho$  (a) and the energy current  $J_u$  (b) as a function of the thermodynamic force  $\mathcal{F}_u$  with  $\mathcal{F}_\rho = 0$ . The negative particle current  $J_\rho$  indicates ICC. The system size is  $L = 20$ . (c) and (d) are the same as (a) and (b), respectively, but for the currents as a function of the thermodynamic force  $\mathcal{F}_\rho$  (with  $\mathcal{F}_u = 0$ ). Here ICC is indicated by the negative energy current  $J_u$ .

Next, we study the role the interactions play in generating ICC. To this end, we investigate how currents depend on the potential barrier. For example, in Fig. 4(a), the results for  $J_\rho$  with  $\mathcal{F}_u > 0$  and  $\mathcal{F}_\rho = 0$  is given. It shows that as  $h \rightarrow 0$ , i.e., when the interactions tend to vanish,  $J_\rho$  increases and turns to be positive, indicating that interactions are necessary to obtain ICC. On the other hand, in the limit  $h \rightarrow \infty$ , when the particles tend to collide elastically without passing through each other, the ICC current decays. Therefore, allowing the particles passing through each other is a crucial element of the interactions for inducing ICC in our system [20].

In the linear response regime, the currents are related to the thermodynamic forces as [21, 22]

$$\begin{pmatrix} J_\rho \\ J_u \end{pmatrix} = \begin{pmatrix} \mathcal{L}_{\rho\rho} & \mathcal{L}_{\rho u} \\ \mathcal{L}_{u\rho} & \mathcal{L}_{uu} \end{pmatrix} \begin{pmatrix} \mathcal{F}_\rho/L \\ \mathcal{F}_u/L \end{pmatrix}, \quad (4)$$

where  $\mathcal{L}_{ij}$  ( $i, j = \rho, u$ ) are the Onsager kinetic coefficients. For the general case where the currents are positive for positive forces,  $\mathcal{L}_{ij} > 0$ . However, thermodynamics does not forbid the cross coefficients to be negative. As shown in Fig. 4(b), our model exhibits such an unusual feature, and indeed, it is when  $\mathcal{L}_{\rho u} < 0$  that ICC occurs in the linear response regime.

The fact that  $\mathcal{L}_{\rho u} < 0$  can be understood as follows. If we set  $\mathcal{F}_\rho = 0$  and  $\mathcal{F}_u > 0$ , the probability for two particles to cross each other is higher when the light particle (a rod) is closer to the hot end and the heavy particle (a

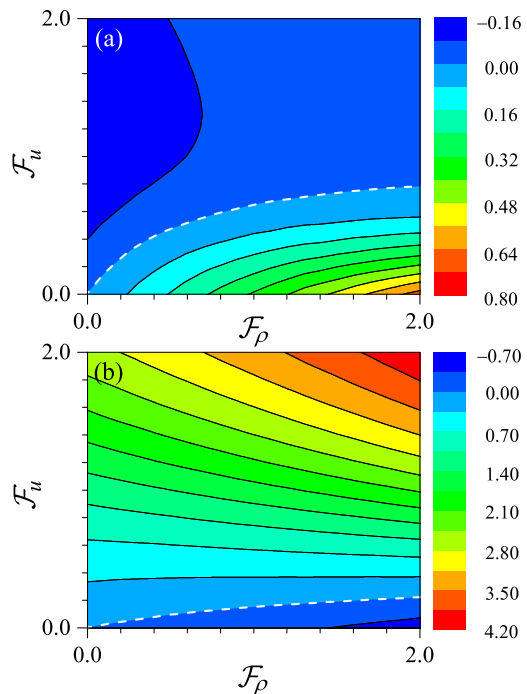


FIG. 3. The particle current  $J_\rho$  (a) and the energy current  $J_u$  (b) as a function of the thermodynamic forces  $\mathcal{F}_u$  and  $\mathcal{F}_\rho$ . ICC occurs in  $J_\rho$  when the thermodynamic forces fall in the area above the white dashed curve in (a) while it occurs in  $J_u$  when the thermodynamic forces fall in the area below the white dashed curve in (b). The system size is  $L = 20$ .

bullet) is closer to the cold end. In this case, the relative velocity of the two particles is on average higher than in the opposite configuration, hence crossing is more likely. This creates an unbalance in the particle density for the two species, with the rods staying preferably closer to the cold side and the bullets close to the hot side (such an unbalance develops to a phase separation in the far-from-equilibrium regime). As only bullets exchange with the reservoir, an average flow of bullets from the cold to the hot reservoir will form, i.e.,  $J_\rho < 0$ . This in turn implies  $\mathcal{L}_{\rho u} < 0$  [see Eq. (5)] in the linear response regime.

Now we state two properties of ICC in our model. First, numerical data on the size dependence of ICC (see Sec. I of the Supplemental Material [23]) show that, for fixed driving forces, ICC first becomes stronger and then saturates with increasing system size, in both the linear response regime and beyond. These data provide a clear indication for the existence and relevance of ICC in our model in the limit of large system size.

Second, for a large, fixed system size, a phase separation occurs when driving forces exceed certain values, causing a dramatic enhancement of the ICC effect. As an example, in Fig. 5(a) is shown the particle current  $J_\rho$  driven by  $\mathcal{F}_u$  with  $\mathcal{F}_\rho = 0$  for a large system size  $L = 1280$ . It can be seen that, below a turning

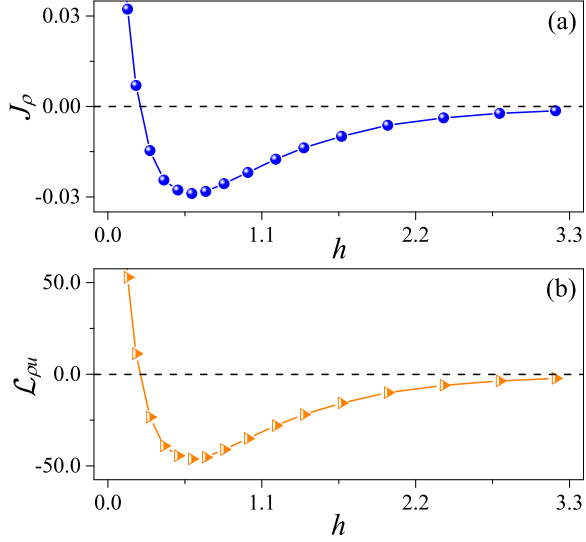


FIG. 4. The dependence on the interaction potential barrier  $h$  of (a) the particle current  $J_\rho$  and (b) the Onsager cross coefficient  $\mathcal{L}_{\rho u}$ . The thermodynamic forces are  $\mathcal{F}_\rho = 0$  and  $\mathcal{F}_u = 0.1$ , respectively, and the system size is  $L = 160$ .

point  $\mathcal{F}_u^{(c)} \approx 0.4$ ,  $|J_\rho|$  increases with  $\mathcal{F}_u$  slowly. Instead, for  $\mathcal{F}_u > \mathcal{F}_u^{(c)}$ , when the phase separation takes place (see below),  $|J_\rho|$  increases with  $\mathcal{F}_u$  sharply. This abrupt change is even more evident in the rescaled particle current  $\tilde{\mathcal{L}}_{\rho u} \equiv J_\rho L / \mathcal{F}_u$  [the inset of Fig. 5(a)]. This quantity, which tends to  $\mathcal{L}_{\rho u}$  in the linear response regime  $\mathcal{F}_u \rightarrow 0$ , first decays (in absolute value) for  $\mathcal{F}_u < \mathcal{F}_u^{(c)}$  and then rapidly increases when  $\mathcal{F}_u > \mathcal{F}_u^{(c)}$ .

To illustrate the phase separation at  $\mathcal{F}_u = \mathcal{F}_u^{(c)} \approx 0.4$ , we show in Fig. 5(b) the averaged particle mass,  $\langle m(x) \rangle$ , for all the particles that pass a certain position  $x$ . We can see that, for small driving force,  $\langle m(x) \rangle$  is almost uniform except that at the left end it is a bit higher. Hence the two types of particles are overall uniformly mixed. As the driving force is strengthened, the left end of the curve lifts higher, suggesting that bullets (of mass  $\mathcal{M}_1 = 1$ ) tend to accumulate at the left end and rods (of mass  $\mathcal{M}_2 = 0.5$ ) are pushed to the right. When the driving force reaches the critical value, the left end is exclusively occupied by the bullets. For even stronger driving force, a domain of pure bullet particles emerges at the left end, and the rods are brought out of contact with the left reservoir completely, indicating that a critical transition in the system's structure has occurred. The change in structure is a self-organization behavior to adaptively respond to the external forces, which recalls that observed in the system's heat conduction behavior [11]. We also note that ANM was observed in Ref. [1] for Brownian particles, as a consequence of particle-particle attractive interactions and of a kind of self-organization in the system. While in Ref. [1] the dynamics is ruled by a Markovian master

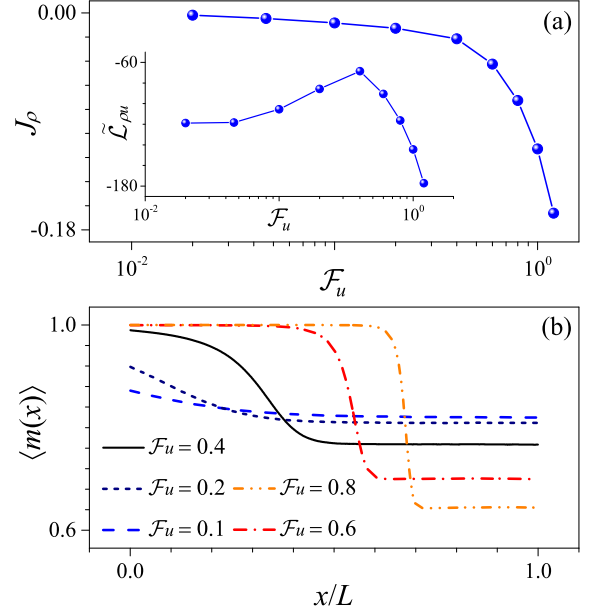


FIG. 5. (a) The particle current  $J_\rho$  as a function of the thermodynamic force  $\mathcal{F}_u$  with  $\mathcal{F}_\rho = 0$ . The system size is  $L = 1280$ . The inset shows  $\tilde{\mathcal{L}}_{\rho u} \equiv J_\rho L / \mathcal{F}_u$ . (b) The average mass of all particles passing a given point  $x$  along the system. The five curves correspond to the middle five points shown in panel (a).

equation and only the particle flow is considered; in our case we consider coupled flows for a Hamiltonian dynamics.

In summary, we have shown that ICC can take place in a 1D, interacting Hamiltonian system, in either the particle or the energy current. The effect is observed both within linear response and beyond and is rooted in the self-organization in response to the applied forces, up to complete phase separation in the far-from-equilibrium regime, where ICC is greatly enhanced. Our results raise the question of what the general conditions for ICC are and if other mechanisms different from self-organization exist. It might be also interesting to explore possible new effects that negative Onsager cross coefficients may induce [29, 30], of which those on thermoelectricity [24–28] might be of particular interest [31]. For instance, one could, in principle, design a thermoelectric circuit [24] with only one kind of electric carrier rather than alternating  $p$ - and  $n$ -doped semiconductors as in a thermocouple. The opposite response to a temperature difference could be obtained by alternating a channel with standard response to applied thermodynamic forces and a channel that exhibits ICC.

We acknowledge support by the NSFC (Grants No. 11535011 and No. 11335006) and by the INFN through the project QUANTUM. The computational resources utilized in this study were provided by the Shanghai Supercomputer Center.

## Supplemental Material: Inverse Currents in Hamiltonian Coupled Transport

Here we provide more analysis of ICC in our model. For all the numerical results presented, the parameters adopted in simulations are the same as in the main text.

### I. Dependence on system size

In Fig. 6, the dependence of the currents  $J_\rho$  and  $J_u$  on the thermodynamic forces  $\mathcal{F}_\rho$  and  $\mathcal{F}_u$  is shown for various system sizes. It can be seen that, in general, the currents drop as the system size increases. But, however, the relevance of ICC is not decreasing. Indeed, as shown in Fig. 7, at a given force  $\mathcal{F}_u$  or  $\mathcal{F}_\rho$ , as the system size increases, both the negative ratio  $J_\rho/J_u$  (at  $\mathcal{F}_\rho = 0$ ) and  $J_u/J_\rho$  (at  $\mathcal{F}_u = 0$ ) would increase first (in absolute value) and then tend to saturate.

### II. Thermoelectric implications

In the linear response regime, the currents are related to the thermodynamic forces as [21, 22]

$$\begin{pmatrix} J_\rho \\ J_u \end{pmatrix} = \begin{pmatrix} \mathcal{L}_{\rho\rho} & \mathcal{L}_{\rho u} \\ \mathcal{L}_{u\rho} & \mathcal{L}_{uu} \end{pmatrix} \begin{pmatrix} \mathcal{F}_\rho/L \\ \mathcal{F}_u/L \end{pmatrix}, \quad (5)$$

where  $\mathcal{L}_{ij}$  ( $i, j = \rho, u$ ) are the Onsager kinetic coefficients.

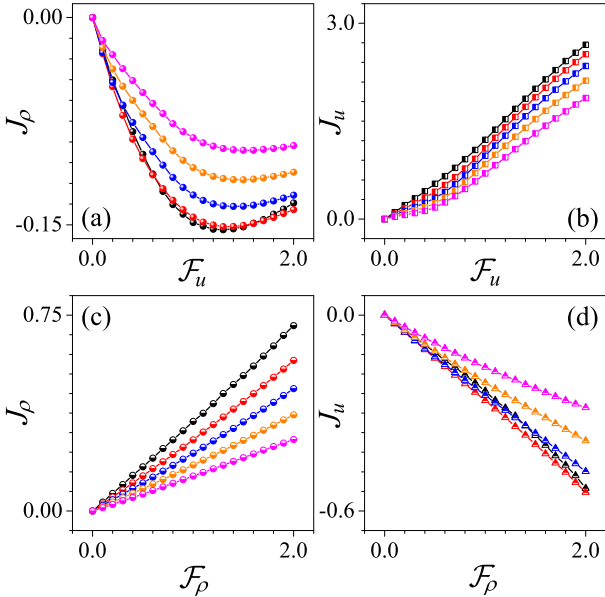


FIG. 6. The same as Fig. 2 in the main text, but for five different system sizes. In each panel, the black, red, blue, orange, and magenta curve are for, respectively, the system size of  $L = 20, 40, 80, 160$ , and  $320$ .

In our system, if the bullet particles are charge carriers, then the electric conductivity  $\sigma$ , the thermal conductivity  $\kappa$ , and the Seebeck coefficient  $S$  of the system are connected with  $\mathcal{L}_{ij}$  ( $i, j = \rho, u$ ) as

$$\sigma = \frac{e^2}{T} \mathcal{L}_{\rho\rho}, \quad \kappa = \frac{1}{T^2} \frac{\det \mathcal{L}}{\mathcal{L}_{\rho\rho}}, \quad S = \frac{1}{eT} \left( \frac{\mathcal{L}_{\rho u}}{\mathcal{L}_{\rho\rho}} - \mu \right), \quad (6)$$

where  $e$  is the charge of a bullet particle and  $\det \mathcal{L}$  denotes the determinant of the matrix of Onsager kinetic coefficients. The thermoelectric figure of merit  $ZT$  can be expressed in terms of these transport coefficients as [24]

$$ZT = \frac{\sigma S^2}{\kappa} T. \quad (7)$$

Thermodynamics imposes  $ZT \geq 0$ , with the efficiency of heat to work conversion  $\eta = 0$  when  $ZT = 0$  and  $\eta \rightarrow \eta_C$  when  $ZT \rightarrow \infty$ ,  $\eta_C$  being the Carnot efficiency.

In Fig. 8, the system size dependence of the Onsager kinetic coefficients is provided. It can be seen that the absolute value of all Onsager coefficients increases with the system size. Moreover, the cross-coefficient  $\mathcal{L}_{\rho u}$  is negative ( $\mathcal{L}_{u\rho} = \mathcal{L}_{\rho u}$  due to the Onsager reciprocal relations [21]). For simulations, the charge  $e$  is set to be unity throughout.

The size dependence of the transport coefficients and  $ZT$  is shown in Fig. 9. It can be seen that while the Seebeck coefficient is negative and saturates to a certain value, the electric conductivities  $\sigma$  and the heat conductivity  $\kappa$  keep growing, but at different rates so that  $ZT$  increases monotonically. Extrapolation of these results to

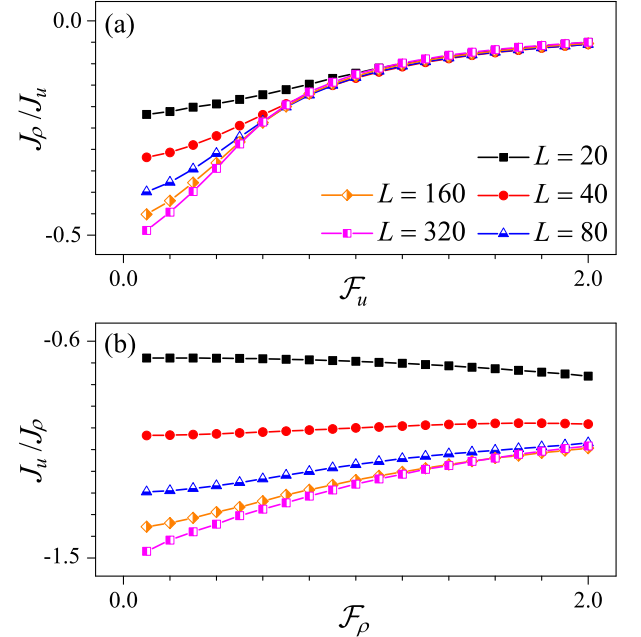


FIG. 7. (a) Ratio  $J_\rho/J_u$  versus the thermodynamic force  $\mathcal{F}_u$  (at  $\mathcal{F}_\rho = 0$ ) and (b)  $J_u/J_\rho$  versus  $\mathcal{F}_\rho$  (at  $\mathcal{F}_u = 0$ ) for different system sizes. Legends in panel (a) also apply to panel (b).



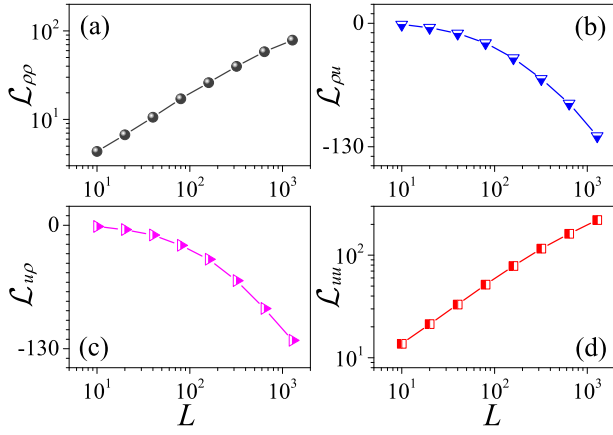


FIG. 8. The dependence of the Onsager kinetic coefficients on the system size. The Onsager kinetic coefficients are evaluated based on Eq. (5) by computing the currents with  $(\mathcal{F}_\rho, \mathcal{F}_u)$  being  $(0, 0.04)$  and  $(0.04, 0)$ , respectively.

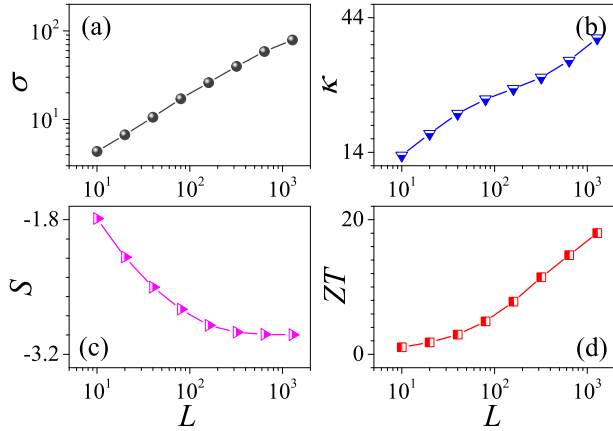


FIG. 9. The dependence of the transport coefficients and  $ZT$  on the system size in the linear response regime based on the computed Onsager kinetic coefficients presented in Fig. 8.

the thermodynamic limit would imply that the Carnot efficiency would be achieved in that limit, similar to other momentum conserving systems [25–28].

---

[1] B. Cleuren and C. Van den Broeck, *Europhys. Lett.* **54**, 1 (2001); *Phys. Rev. E* **65**, 030101(R) (2002); C. Van den Broeck, B. Cleuren, R. Kawai, and M. Kambon, *Int. J. Mod. Phys. C* **13**, 1195 (2002).  
[2] R. Eichhorn, P. Reimann, and P. Hänggi, *Phys. Rev. Lett.* **88**, 190601 (2002); *Phys. Rev. E* **66**, 066132 (2002).  
[3] D. Reguera, A. Luque, P. S. Burada, G. Schmid, J. M. Rubi, and P. Hänggi, *Phys. Rev. Lett.* **108**, 020604 (2012).  
[4] A. Ślapiak, J. Łuczka, P. Hänggi, and J. Spiechowicz *Phys. Rev. Lett.* **122**, 070602 (2019).  
[5] P. K. Ghosh, P. Hänggi, F. Marchesoni, and F. Nori,

*Phys. Rev. E* **89**, 062115 (2014).  
[6] A. Sarracino, F. Cecconi, A. Puglisi, and A. Vulpiani *Phys. Rev. Lett.* **117**, 174501 (2016).  
[7] B. J. Keay, S. Zeuner, S. J. Allen, Jr., K. D. Maranowski, A. C. Gossard, U. Bhattacharya, and M. J. W. Rodwell, *Phys. Rev. Lett.* **75**, 4102 (1995).  
[8] A. Ros, R. Eichhorn, J. Regtmeier, T. T. Duong, P. Reimann, and D. Anselmetti, *Nature* **436**, 928 (2005).  
[9] J. Nagel, D. Speer, T. Gaber, A. Sterck, R. Eichhorn, P. Reimann, K. Ilin, M. Siegel, D. Koelle, and R. Kleiner, *Phys. Rev. Lett.* **100**, 217001 (2008).  
[10] J. Cividini, D. Mukamel, and H. A. Posch, *J. Phys. A: Math. Theor.* **51**, 085001 (2018).  
[11] J. Wang and G. Casati, *Phys. Rev. Lett.* **118**, 040601 (2017).  
[12] E. H. Lieb and W. Liniger, *Phys. Rev.* **130**, 1605 (1963); E. H. Lieb, *Phys. Rev.* **130**, 1616 (1963).  
[13] G. Casati, *Found. Phys.* **16**, 51 (1986).  
[14] A. Garriga, J. Kurchan, and F. Ritort, *J. Stat. Phys.* **106**, 109 (2002).  
[15] C. Mejía-Monasterio, H. Larralde, and F. Leyvraz, *Phys. Rev. Lett.* **86**, 5417 (2001); H. Larralde, F. Leyvraz, and C. Mejía-Monasterio, *J. Stat. Phys.* **113**, 197 (2003).  
[16] K. Saito, G. Benenti, and G. Casati, *Chem. Phys.* **375**, 508 (2010).  
[17] J. L. Lebowitz and H. Spohn, *J. Stat. Phys.* **19**, 633 (1978); R. Tehver, F. Toigo, J. Koplik, and J. R. Banavar, *Phys. Rev. E* **57**, R17 (1998).  
[18] The existence of ICC does not depend on the coupling between the rod particles and the reservoirs. For example, ICC is verified to exist even if the rod particles are insulated from the reservoirs by setting their reflected velocity unchanged but the direction.  
[19] G. Casati and T. Prosen, *Phys. Rev. E* **67**, 015203(R) (2003).  
[20] This finding is also supported by the results of ICC current  $J_u$  when  $\mathcal{F}_u = 0$  but  $\mathcal{F}_\rho > 0$  and other cases where both thermodynamic forces are nonzero.  
[21] H. B. Callen, *Thermodynamics and an Introduction to Thermostatistics* (2nd ed.) (John Wiley & Sons, New York, 1985).  
[22] S. R. de Groot and P. Mazur, *Nonequilibrium Thermodynamics* (North-Holland, Amsterdam, 1962).  
[23] See Supplemental Material for numerical analysis on the system-size dependence of ICC and on the thermoelectric implications of ICC in our model, which includes Refs. [21, 22, 24–28].  
[24] G. Benenti, G. Casati, K. Saito, and R. S. Whitney, *Phys. Rep.* **694**, 1 (2017).  
[25] G. Benenti, G. Casati, and J. Wang, *Phys. Rev. Lett.* **110**, 070604 (2013).  
[26] G. Benenti, G. Casati, and C. Mejía-Monasterio, *New J. Phys.* **16**, 015014 (2014).  
[27] S. Chen, J. Wang, G. Casati, and G. Benenti, *Phys. Rev. E* **92**, 032139 (2015).  
[28] R. Luo, G. Benenti, G. Casati, and J. Wang, *Phys. Rev. Lett.* **121**, 080602 (2018).  
[29] Note that in the nonequilibrium discrete nonlinear Schrödinger equation a negative Seebeck coefficient was reported [30].  
[30] S. Iubini, S. Lepri, and A. Politi, *Phys. Rev. E* **86**, 011108 (2012).  
[31] Some thermoelectric properties of our model are outlined in Sect. II of the Supplemental Material [23].